JOURNAL OF MATERIALS SCIENCE 19 (1984) 2259–2272

The application of X-ray photoelectron spectroscopy to the study of polymer-to-metal adhesion

Part 2 *The cathodic disbondment of epoxy coated mild steel*

J. F. WATTS, J. E. CASTLE
Department of Metallurgy and Materials Technology, University of Surrey, Guildford, UK

The delamination of a commercial epoxy coating applied to cathodically protected mild steel has been investigated from both a mechanistic and a kinetic standpoint. X-ray photoelectron spectroscopy shows the locus of failure to be invariant with surface profile, and essentially adhesive in nature. The substrate pretreatment does, however, determine the kinetics of disbondment. A three-stage process for such failure is identified, the rate-controlling step passing from oxide reduction at a defect to the cathodic area exposed, and finally to interfacial path length. A simple relationship is presented to describe the disbondment rate in terms of this interfacial path length. The concept of a critical disbondment velocity for the epoxy mild steel system is proposed. It is shown that oxide reduction is an important precursor to cathodic disbondment for this system.

1. Introduction

It is nowadays general practice amongst the oil and gas industries to protect transmission line pipe with a combination of impressed current cathodic protection, and a high performance organic coating such as a fusion bonded epoxy, to ensure corrosion-free operation. In the majority of cases such a combination proves to be reliable and trouble free in use, but problems can occur around any defects in the organic coating. At such regions rapid delamination of the coating is observed, a condition which is exacerbated by the presence of the cathodic potential; hence the phenomenon is widely referred to as cathodic disbondment (or delamination).

In this paper, we report an investigation into the kinetics of disbondment for a fusion-bonded epoxy coating applied to mild steel substrates pretreated to give a wide range of surface profiles. The interfacial chemistry of cathodic disbondment has been studied using X-ray photoelectron spectroscopy (XPS). By obtaining spectra at high resolution and then separating the chemical states by a computer curve fitting process, it has proved possible to gain an insight into the behaviour of the substrate oxide; both at the time of disbondment and during the subsequent advancement of the disbondment front.

By combining the XPS results with the kinetic data it has been possible to postulate a comprehensive model for the failure of this system.

2. Experimental procedure

2.1. Substrate pretreatment

Thin (1.5 mm) mild steel panels measuring approximately 100 mm x 75 mm were used to allow for routine preparation of specimens for XPS analysis. The chemical analysis of this material is given in Table I. Prior to coating they were pretreated in one of the following ways, chosen to give a range of surface topographies:

1. grit blasting with G12 chilled iron grit.
2. abrasion with grade F engineers emery cloth (120 grit);
3. agitation in a commercial alkali cleaner*;
4. polish to a mirror finish with 1 μm diamond paste.

The roughness average (R_a) values of the sub-

*Solventol 5024 ex EFCO Ltd, Woking UK.

0022–2461/84 $03.00 + .12

TABLE I Chemical analysis (wt%) of steel substrate alloy

C	Si	Mn	P	S	Fe
0.13	0.17	0.46	0.023	0.015	balance

strates after pretreatment were recorded using a Rank Hobson Talysurf 10 stylus profilometer.

2.2. Application of the epoxy powder coating

The epoxy coating used in this study is manufactured by 3M under the product designation 206N. Samples of the thickness suitable for insertion in the electron spectrometer (i.e. about 1.5 mm) have inadequate thermal mass. Prior to application, the panels were clamped to a 6 mm steel plate to ensure adequate thermal mass and placed in an air oven at 240° C for 30 min giving the mild steel a characteristic golden colouration. Following powder spraying, using a compressed air gun, panels were returned to the oven for a further 2 min to cure. They were then quenched in cold water.

2.3. Cathodic disbondment tests

These tests were carried out according to the relevant British Gas Specification [1] shown schematically in Fig. 1. A central, initiating defect was made in each panel with a twist drill. All tests were carried out at a cathodic potential of −1500 mV (versus SCE) using 0.52 M NaCl solution. To reduce evaporation from the cells they were covered with glass slides. The potential was checked two or three times a week.

After polarization for the required time, the test was stopped, the electrolyte ring removed from the test panel, which was washed with distilled water and stored in a vacuum desiccator for at least 24 h. The extent of disbondment was assessed by cutting the coating radially outwards from the defect. Specimens were then cut from both substrate and coating for XPS analysis.

2.4. Surface analysis

X-ray photoelectron spectra were recorded using a V.G. Scientific ESCA 3 Mk II with Al$K\alpha$ radiation ($h\nu$ = 1486.6 eV) at a pass energy of 50 eV. The vacuum in the analyser chamber during analysis was approximately 5×10^{-10} torr. During acquisition, and for subsequent data analysis, the spectrometer was controlled by a VG 3040 datasystem based on a DEC PDP8e computer. Quantification of the XPS results was achieved using the appropriate sensitivity factors, mainly those of Jorgensen and Berthou [2].

Ion bombardment was carried out to remove surface layers using a VG Scientific AG2 ion gun. A beam energy of 3 kV and a focus potential of 1.5 kV in a residual argon pressure of 10^{-6} torr was employed.

3. Results

3.1. Characteristics of the uncoated steel substrate

Previous work from this laboratory [3] has shown that the different methods of surface treatment leave the steel surface in quite different states, the alkali-cleaned surface having a much higher level of adventitious material. After heat treatment at 240° C prior to coating, adsorbed water and a large proportion of aliphatic carbon is lost, and the surface chemistries of the substrate surfaces are essentially the same for the different modes of surface treatment.

The surface topographies of the substrates were characteristic of the pretreatments employed. Talysurf traces for grit-blasted, alkali-cleaned and emery-abraded steel are shown in Fig. 2 together with their R_a values. For the diamond-polished panel an R_a value of 0.05 μm was recorded.

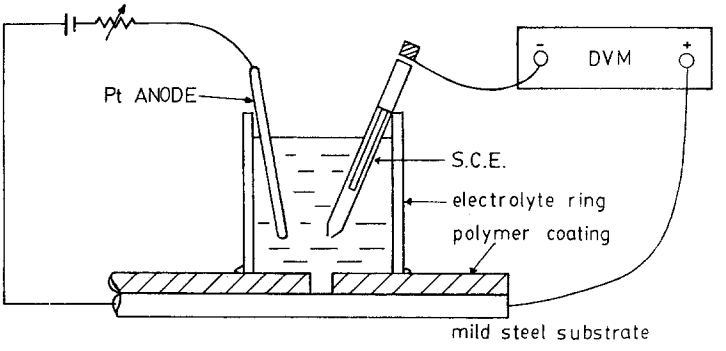

Figure 1 Schematic diagram of cathodic disbondment test.

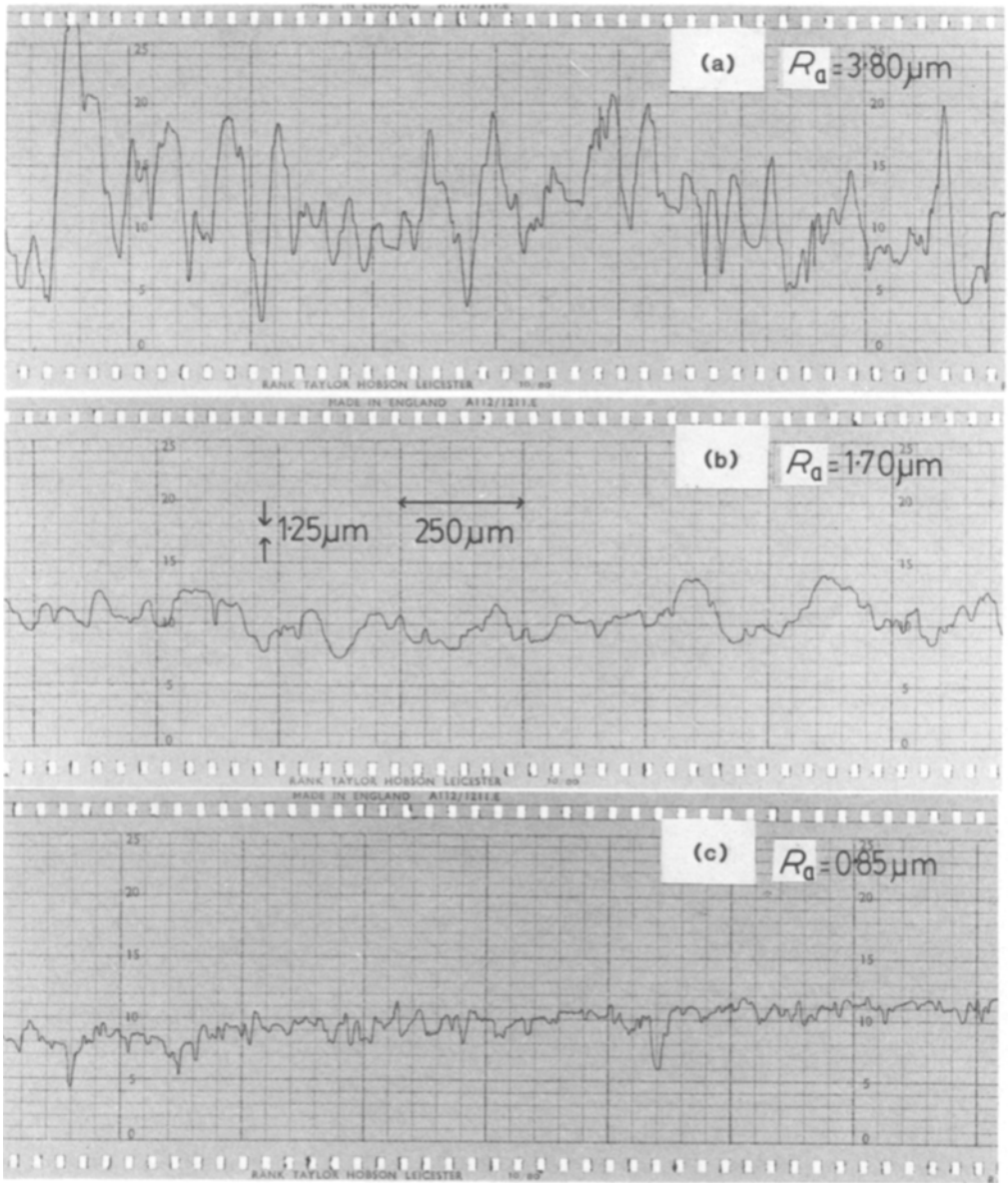

Figure 2 Talysurf traces for mild steel following (a) grit blasting, (b) alkali cleaning, and (c) emery abrasion.

3.2. Kinetics of cathodic disbondment

The kinetics of disbondment, i.e. disbondment area as a function of time are shown in Fig. 3. The area was calculated from the exposed metal area after cathodic polarization of the coated panel, which invariably approximated to a circle, less an allowance of 10 mm^2 for the initial defect.

By taking the slope of each curve of Fig. 3 it is possible to deduce a disbondment rate for each substrate pretreatment. This value is plotted as a function of surface profile in Fig. 4.

Such a treatment of disbondment kinetics assumes that the rate of delamination is constant, although this assumption would not be justified on the basis of the relatively few data, especially with their added bias towards long exposure times. It has been reported, in fact [4], that for epoxy coatings on steel substrates the rate of delamination is not constant. To investigate the initial stages of disbondment further, a series of diamond-polished, coated panels were cathodically polarized and the extent of disbondment recorded after various exposure times of up to 20 days. Inspection of the data shows it to fit a logarithmic rather than a linear dependence on time during the initial exposure period (Fig. 5).

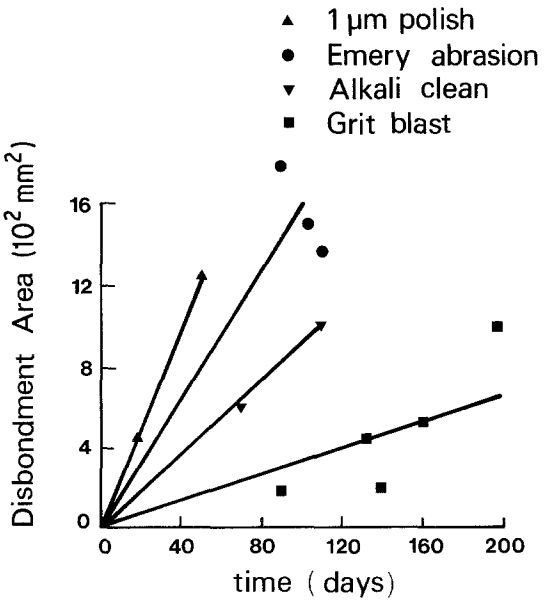

Figure 3 Extent of cathodically disbonded area as a function of time.

By combining the data of Fig. 5 with that of Fig. 3 and plotting it on a linear scale (Fig. 6) it seems that there is a marked change in the rate of disbondment at a point which is strongly dependent on surface profile. In Fig. 6 these times at which the change from logarithmic to linear rate occur have been labelled t_1, t_2, t_3, t_4, for in turn, grit-blasted, alkali-cleaned, emery-abraded and polished substrate. The significance of these values in terms of the mechanism of disbondment will be considered in Section 4.

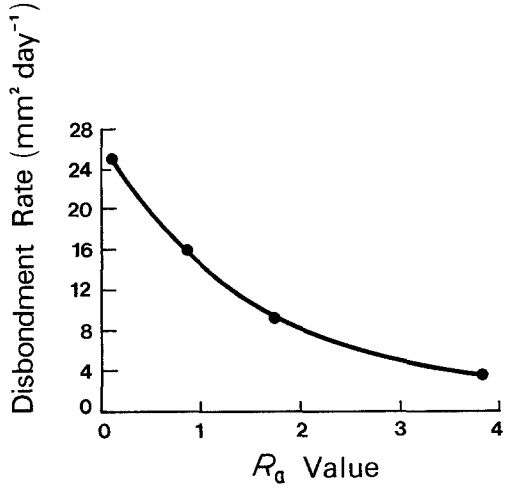

Figure 4 Disbondment rate as a function of substrate surface profile.

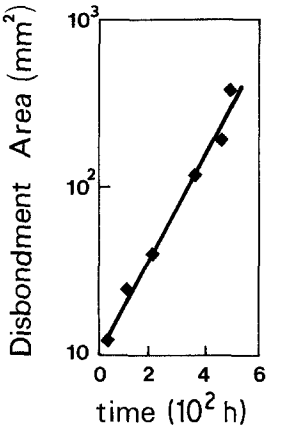

Figure 5 Disbondment kinetics for a series of diamond-polished, coated panels.

3.3. Oxide reduction during disbondment

One feature, characteristic of all test panels irrespective of surface treatment is the development of a silver grey halo around the defect. This is shown in Fig. 7 for diamond-polished substrates polarized for 2 and 19 days. The dimensions of the halo are independent of exposure time and thus for the 2-day test, most of the disbonded area is silver in colour. For the longer term test the silver halo is a relatively small proportion of the disbonded area which mostly shows the darker colouration of the thickened oxide (brought about during the pre-heat prior to coating).

Although these halos tended to be of constant size, the extent did vary with defect geometry. One panel, where the defect sides were more bevelled than usual, showed an abnormally large silver region and it was possible to remove a specimen from this zone for surface analysis. The surface composition as determined by XPS is given in Table II. The Fe2p3/2 spectrum (Fig. 8) is of interest as a metallic iron component can be seen along with the more usual iron (III) contribution.

The low levels (in surface analysis terms) of carbon and nitrogen shows the failure to be truly adhesive in nature. The presence of metallic iron in the spectrum shows the oxide thickness to have been greatly reduced accounting for the colour change from golden to metallic silver.

TABLE II Surface composition (at%) by XPS, of the halo region

C	O	N	Fe	Na	Cl
28.0	57.0	0.4	13.0	1.3	0.7

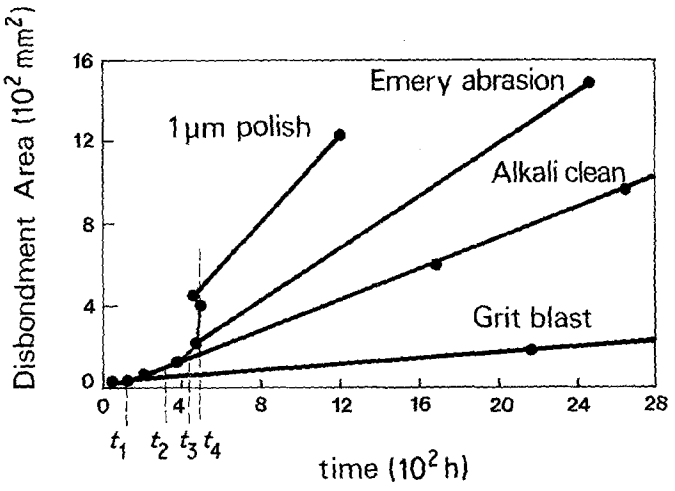

Figure 6 Overall scheme for the kinetics of disbondment.

3.4. Interfacial chemistry of cathodic disbondment

3.4.1. Elemental composition of the failed interface

Specimens for XPS analysis were cut from each panel following disbondment, in general two or three specimens were cut from both coating and substrate. Following quantification it is possible to compare detailed variations in surface composition with surface pretreatment. As a result of the large data set this is best done graphically, and our preferred method is to plot atomic concentration of a particular element against surface profile (R_a value), for all specimens analysed. Thus it is possible to produce a series of plots which reflect the variation of atomic concentration of an element at the interface. All specimens, both coating and substrate, show an excess of sodium to chloride ions at the interface, indicating under-film alkaline conditions to prevail, as we have observed in previous studies.

Graphs of atomic concentration as a function of surface profile, for substrate carbon, oxygen, and nitrogen and of iron on the coating are presented in Figs. 9a to d. The substrate levels of carbon, oxygen and nitrogen produce curves which

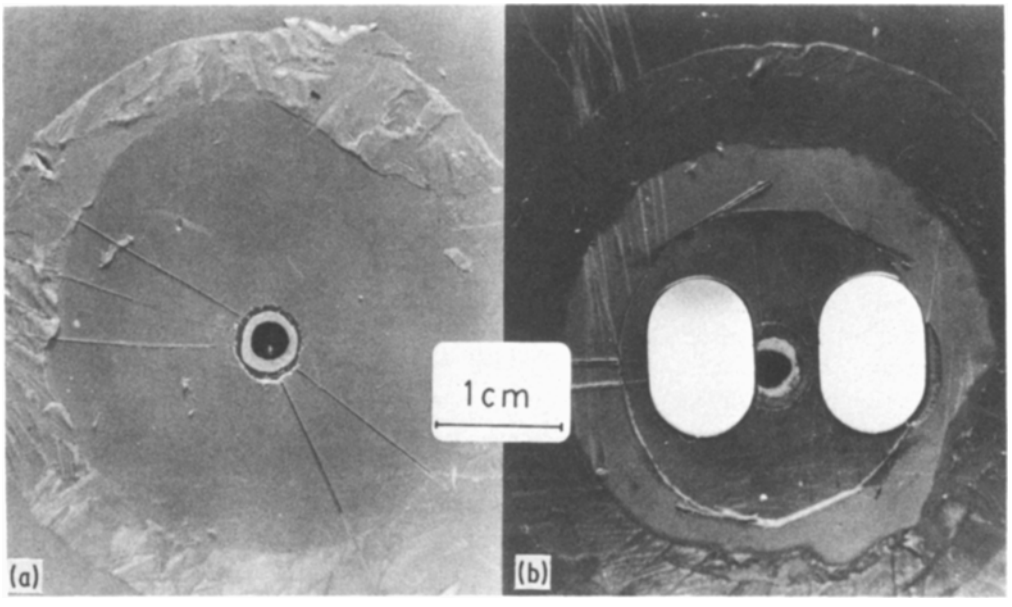

Figure 7 Cathodic disbondment test specimens after (a) 2 and (b) 19 days exposure. Note bright "halo" around the defect.

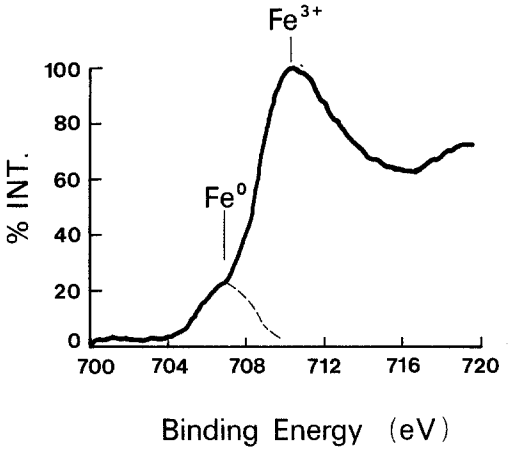

Figure 8 Fe2p3/2 spectrum from "halo" region showing both Fe(0) and Fe(III) components.

show a large amount of scatter on the data points. There is no discernible trend emerging with changing substrate profile. Similar plots can be produced for substrate iron, sodium, and coating nitrogen. It is only the level of iron present on the interfacial surface of the disbonded coating (Fig. 9d), which shows any clear trend. This provides an indication of the manner in which the locus of failure varies as the R_a value increases. As the substrate roughness increases, so the scatter band diverges to higher values, indicating an increasing trend towards cohesive failure of the oxide.

3.4.2. High resolution electron spectra

The quantitative XPS results of Section 3.4.1 enable any differences in interfacial composition to be readily assessed. By applying curve fitting procedures to the high resolution Cls and Ols spectra it is possible to gain more detailed information regarding interfacial chemistry.

3.4.2.1. Carbon ls spectra. All substrate Cls spectra show a subsidiary higher binding energy component as well as the characteristic alkane contribution centred at 285 eV. In the early stages of disbondment (i.e. disbonded surfaces which have been exposed to aqueous solutions for relatively short times), the separation between the alkane line and this minor component is 3.6 eV. This is the polar C=O type material characteristic of a clean oxide surface as we have discussed previously [3]. However, on longer exposures this subsidiary peak is seen to move to a higher binding energy, to give a peak position of 289.2 eV. This is characteristic of a carbonate species. Fig. 10 illustrates this point, showing two carbon ls spectra taken from an emery-abraded panel cathodically polarized for 102 days. Spectrum (a) is taken from the disbonment front, the minor component is centred at 288.6 eV. Spectrum (b) is taken from close to the initiating defect and consequently has been exposed to the saline solution for a much longer time. For this spectrum a minor peak centred at 289.2 eV is seen.

To investigate further the distribution of the carbonate species, depth profiling of a specimen showing this characteristic peak was carried out by argon ion bombardment together with sequential XPS analysis. A Na_2CO_3 standard was also sputter depth profiled under the same standard conditions to assess any ion-induced changes which may arise, as it has been shown that some alkaline earth carbonates decompose on ion bombardment [6].

The change in Cls peak shape with sputter time, for the disbondment specimen is shown in Fig. 11. The lower binding energy peak (C–H carbon), is gradually reduced until after an etch time of 40 min it is of approximately the same intensity as the carbonate contribution. Thereafter, the spectrum shows no change.

In the case of the Na_2CO_3 standard, the CO_3^{2-} component of the Cls spectrum showed no change with sputtering other than the expected reduction in adventitious carbon. The close match of the Cls spectrum from Fig. 11 and the Na_2CO_3 after a short etch time is shown in Fig. 12. The only differences being attributable to better signal-to-noise ratio of the standard; peak position and width match very closely indeed.

The interfacial coating surface consistently shows an asymmetric Cls spectrum. Curve fitting (Fig. 13) shows this to be attributable to epoxy groups (286.6 eV) as well as methyl carbon (285 eV). This feature is in agreement with previous work undertaken on epoxy systems [7, 8] and serves to indicate the absence of severe polymer modification or degradation at the interface during disbondment.

3.4.2.2. Oxygen ls spectra. Interpretation of the Ols spectra excited by Al$K\alpha$ radiation is hampered somewhat by the presence of a minor sodium Auger peak (NaKL_1L_{23}) at a binding energy of 535 to 536 eV

To investigate the position and relative intensity of this Auger line further, a sodium chloride stan-

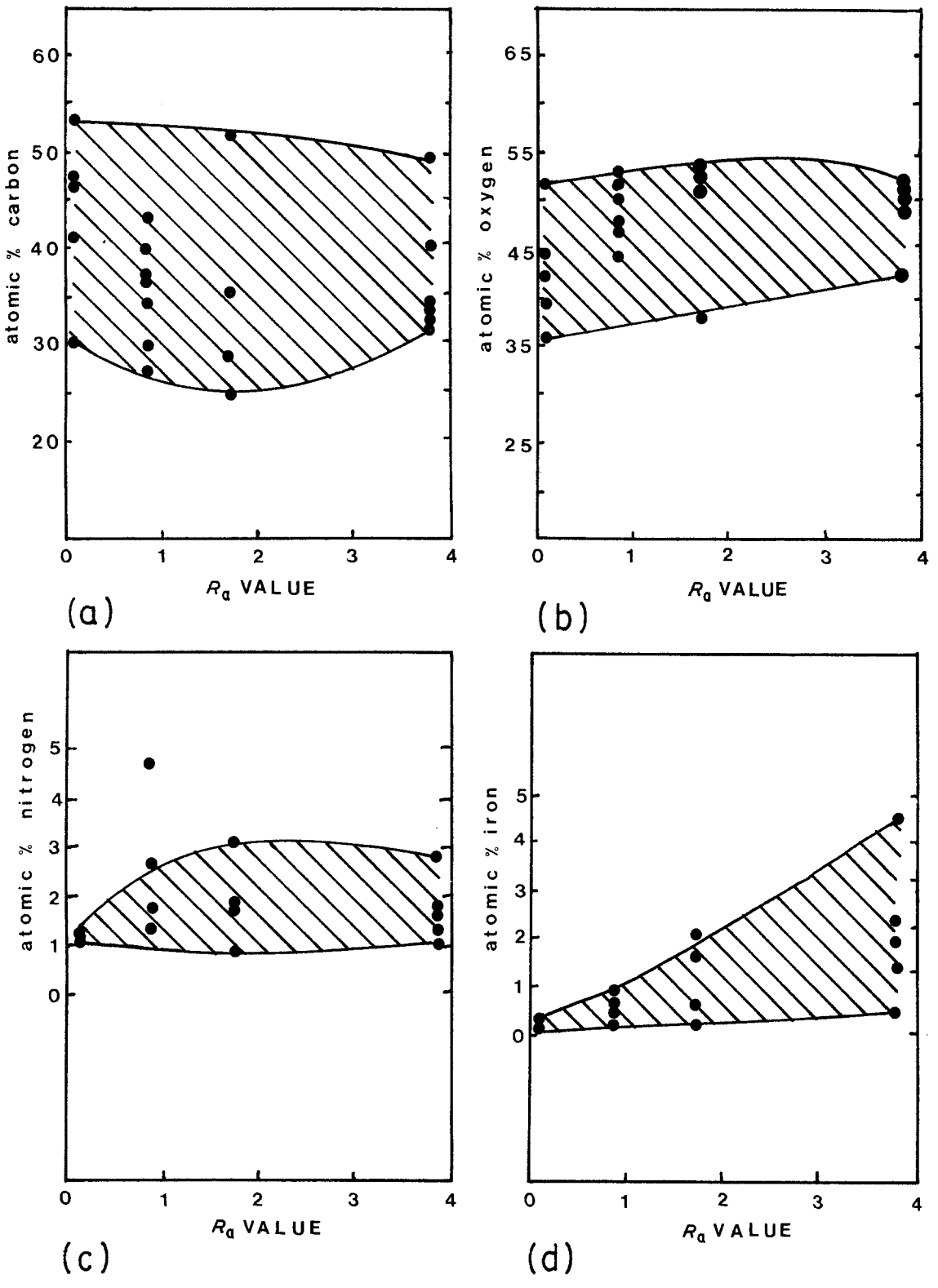

Figure 9 Elemental composition at the disbonded interface: (a) substrate carbon, (b) substrate oxygen, (c) substrate nitrogen, (d) coating iron.

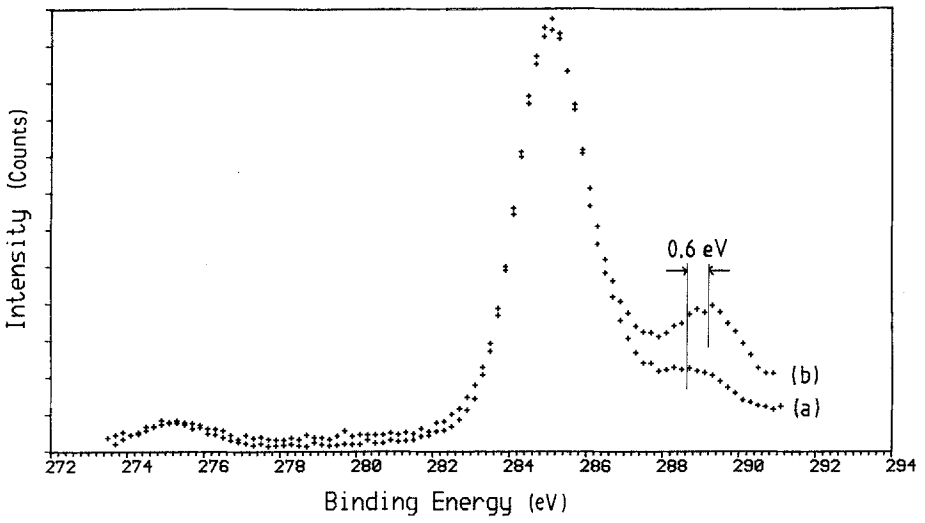

Figure 10 Cls spectra taken from (a) close to the disbondment front, and (b) near the initiating defect, of an emery abraded coated panel exposed for 102 days.

dard was examined in Al$K\alpha$ and Mg$K\alpha$ radiation. No attempt was made to use freshly exposed surface as it was felt that the presence of the Ols line in the resultant spectra would provide a useful internal guide for charge referencing. The Ols spectrum excited by aluminium radiation is shown in Fig. 14a. On switching to magnesium radiation the NaKL_1L_{23} Auger component is removed to another part of the spectrum (Fig. 14b). The relative intensities and peak positions of the photoelectron and Auger peaks, in Al$K\alpha$ radiation, are given in Table III. No attempt has been made to correct for variations in electron inelastic mean free path with energy, or the effect of the attenuating contaminant overlayer.

Throughout this work the Nals peak was used for quantification. Because of the relatively low levels of sodium encountered the effect of the Na$KL_1L_{2,3}$ was, in general, merely an apparent increase in the background signal on the higher binding energy side of the Ols spectrum. It was, however, resolvable as a peak in its own right in some of the spectra, this peak has been observed by other workers and incorrectly ascribed to molecular water [9].

To return now to the disbondment experiments; because of variation of delamination rate with substrate surface profile, and large analysis area of the XPS technique, ($\simeq 25\,mm^2$), any analysis obtained will be an average of the electrochemistry occurring at the tip of the disbondment crevice. In the slowest case (grit-blasted substrate) this may reflect several weeks activity, at best, for the polished substrate, it is a reflection of several days disbondment.

In an effort to further elucidate the changes that occur during disbondment, the Ols spectra from three specimens taken from the same

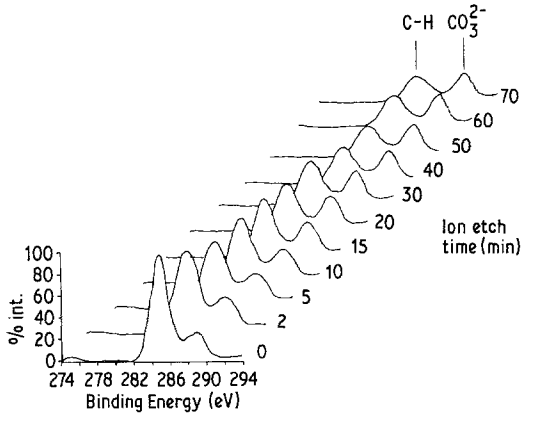

Figure 11 Change of Cls spectrum showing carbonate species, with etch time.

TABLE III Peak position and intensity (relative to Na$KL_{2,3}L_{2,3}$ = 100) of a NaCl standard in Al$K\alpha$ radiation

Origin	Peak position	Relative intensity
Cls	285.0	–
Ols	532.4	–
Na2p	31.1	7.6
Na2s	63.9	15.5
Nals	1072.6	94.2
Na$KL_{2,3}L_{2,3}$	497.4	100
Na$KL_1L_{2,3}$	536.4	25
Cl2p	199.3	–

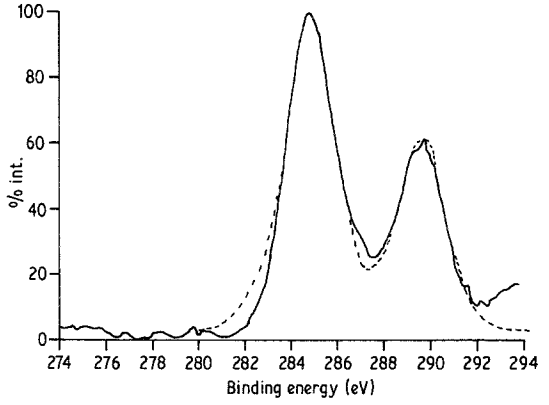

Figure 12 Cls spectra from Fig. 11 (solid line) and Na_2CO_3 standard (dotted line).

diamond-polished panel will be discussed in further detail. This panel was cathodically polarized for 50 days by which time the disbondment front had advanced 20 mm. Specimens were removed from close to the defect, the middle of the disbondment zone and at the tip of the disbondment crevice. All the Cls spectra showed a minor component at 288.6 eV indicative of polar carbon which had not been replaced by carbonate deposits in the relatively short exposure time. The specimen taken from close to the disbondment front is alone in yielding an Ols spectrum centred at 531.8 eV indicating that hydroxyl ions are the major contributors to this peak. Fig. 15 shows curve fitting of this spectrum and it is clear that hydroxide is indeed the major component, the oxide peak being some 40% of the hydroxide. The third component (533.2 eV) is identified as oxygen from epoxy groups. This can be dismissed as a result of cohesive failure of the coating ahead of the disbondment front during specimen preparation. There is also a minor contribution at 535 eV from the sodium Auger transition.

The specimen from close to the defect shows an Ols peak with its main component at 530.2 eV, i.e. oxygen present as an oxide. Peak fitting (Fig. 16) shows a subsidiary peak at 531.8 eV (hydroxide oxygen), approximately 65% of the main peak. The two minor components are a result of the presence of chemically bound water and the sodium Auger peak. The specimen taken from the middle of the disbondment zone was very similar, i.e. the dominant component was the oxide peak with a subsidiary hydroxide contribution.

Thus, notwithstanding the fact that after preheating the surface, oxygen is almost entirely in the oxide state [3], extrapolation of the data obtained above back to the point of disbondment, shows that it is then in the hydroxide state. This view is supported by the sputter depth profile results obtained from an emery-abraded disbondment specimen. Fig. 17 shows a montage of Ols spectra obtained after the ion-bombardment times shown (the Cls spectra have already been discussed, Fig. 11). Initially hydroxide is the major component, but as the hydroxide layer is gradually

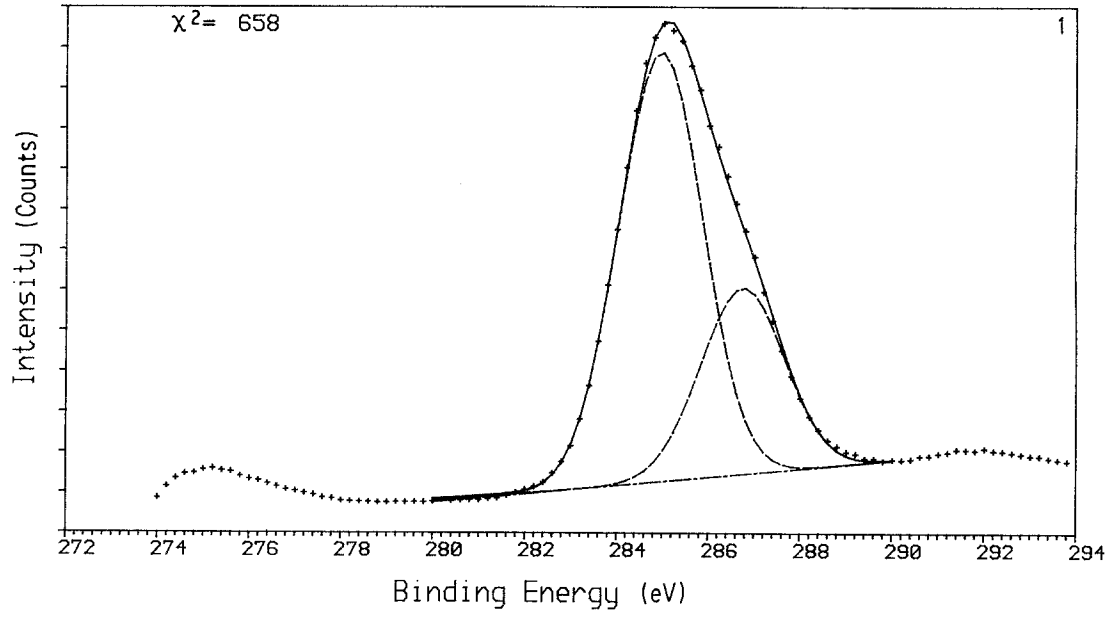

Figure 13 Interfacial coating Cls spectrum. Components due to methyl (left) and epoxy carbon (right).

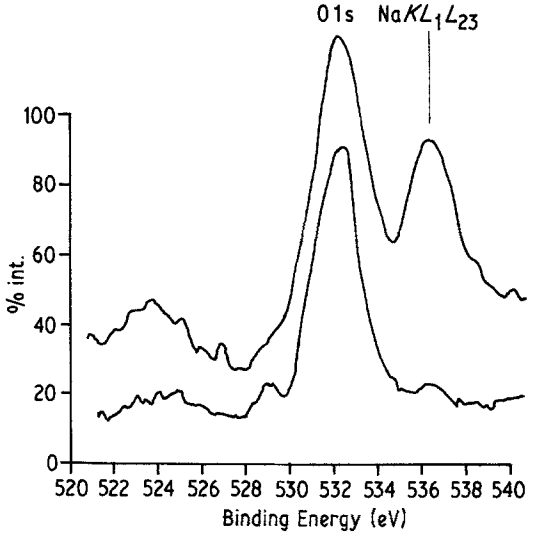

Figure 14 Ols spectral region of NaCl excited by (upper) Al$K\alpha$ X-rays and (lower) Mg$K\alpha$ X-rays. X-ray power was 250 W (12.5 kV at 20 mA) in each case.

removed so an oxide shoulder gradually becomes apparent, after 60 min ion-bombardment it is almost of the same intensity as the hydroxide component, suggesting that the hydroxide is overlying oxide formed during stoving.

3.4.3. Uptake of ions by the polymer film

The level of sodium and chloride ions at the interfacial coating and substrate surfaces has been monitored routinely by XPS. Without exception, there was an excess of sodium over its anion indicating that alkaline, cathodic conditions prevail under the coating during disbondment. This is brought about by the cathodic reduction of oxygen, and is the generally accepted view within the coatings industry and a phenomenon we have observed in previous work [3, 5]. It is not our intention to dwell on this preponderance of sodium ions in this section but merely to use it as a yardstick for the comparison of the uptake of ions by the polymer exposed under a variety of conditions.

In contrast to the interfacial polymer, the outer surface of the disbonded coating shows a large excess of chloride ions (Table IV). To investigate the uptake of ions by the polymer, in the absence of any impressed potential, a piece of free film was soaked in 0.52 M NaCl solution for 7 months. Following washing in distilled water and vacuum dehydration for 24 h, surface analysis was carried out. The results (Table IV) show the level of chlorine to be very low but still in excess of sodium concentration.

To determine the extent of penetration of sodium ions into the bulk of the polymer, a piece of disbonded material was analysed by XPS to assess sodium and chlorine levels and then mounted for cross-sectional analysis by EPMA. The results were obtained by positioning the elec-

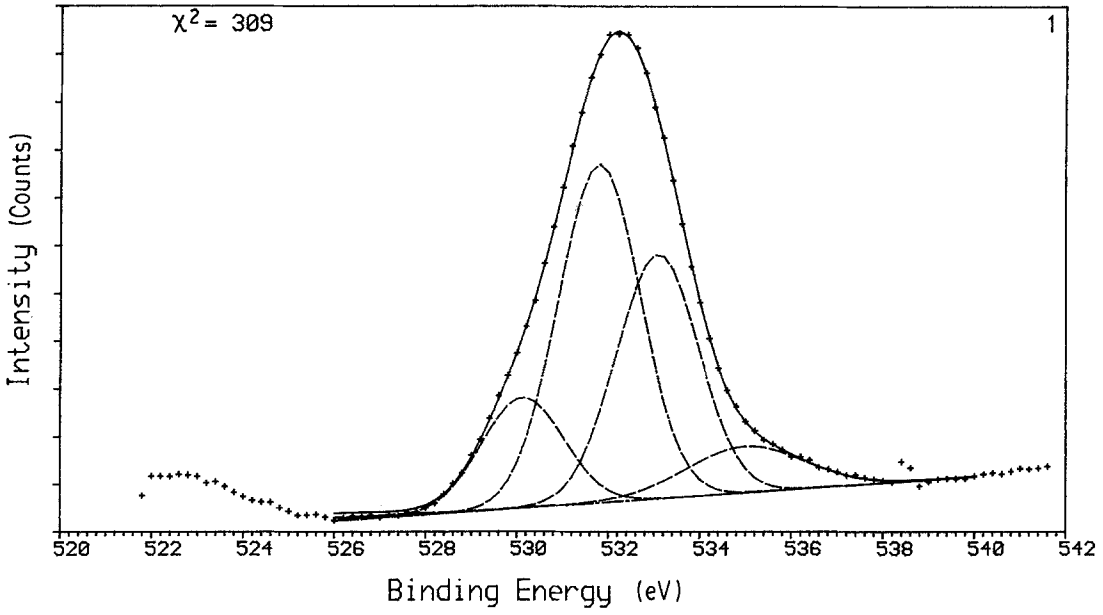

Figure 15 Substrate Ols spectrum from the disbondment front. Components are (left to right) oxide, hydroxide, epoxy, Na*KLL* Auger peak.

TABLE IV XPS analysis (at%) of epoxy films with different histories showing the variation in the level of sodium and chloride ions

Location	C	O	N	Na	Cl	Fe
Interfacial surface*	70.0	22.9	2.2	3.4	0.9	0.6
Outer surface*	62.4	28.3	1.6	0.4	7.3	0
Free film soaked in 0.52 M NaCl	74.3	23.9	1.5	trace	0.3	0

*Cathodicallly polarized.

tron beam at either of the free surfaces or at the centre of the film, and then rotating the crystal spectrometer through the Na$K\alpha$, $K\beta$ region of the spectrum. Fig. 18 shows the presence of sodium both at the outer and interfacial surfaces (also present in the complementary XPS results) but sodium is absent from the bulk of the film. The fact that EPMA can detect sodium (the analysis area in the polymer, allowing for beam spreading, may be as large as 20μm), shows that it has diffused micrometres into the film, from both sides, although not penetrated it completely.

4. Discussion

Although the kinetic data of Section 3.2 show the rate of cathodic disbondment to be highly dependent on substrate surface profile, the interface analyses of Fig. 9 show that, within experimental scatter, interface composition does not vary with substrate pre-treatment. It is therefore reasonable to assume that the chemical mechanism of disbondment of epoxy on mild steel is independent of surface profile. In this context, it should be noted that the surface chemistries of the substrates were remarkably similar after the pre-heat in air prior to coating. The level of nitrogen on the failed interfaces is most probably a result of adsorption from test solution, a phenomenon we have routinely observed in XPS analysis of aqueous corrosion specimens. Although the epoxy is of the amine-cured variety the concentration of nitrogen detected in the free film is $\simeq$ 1%, the lower limit of the scatter band of Fig. 9c.

The surface analysis results show that failure is essentially adhesive. Although some iron is transferred to the polymer, and the amount increases with surface roughness, it remains a trivial component in the locus of failure. This is consistent with the fracture of protruding oxide asperities.

Having established that the mode of failure is invariant with surface profile it is informative to consider the high-resolution spectra from the

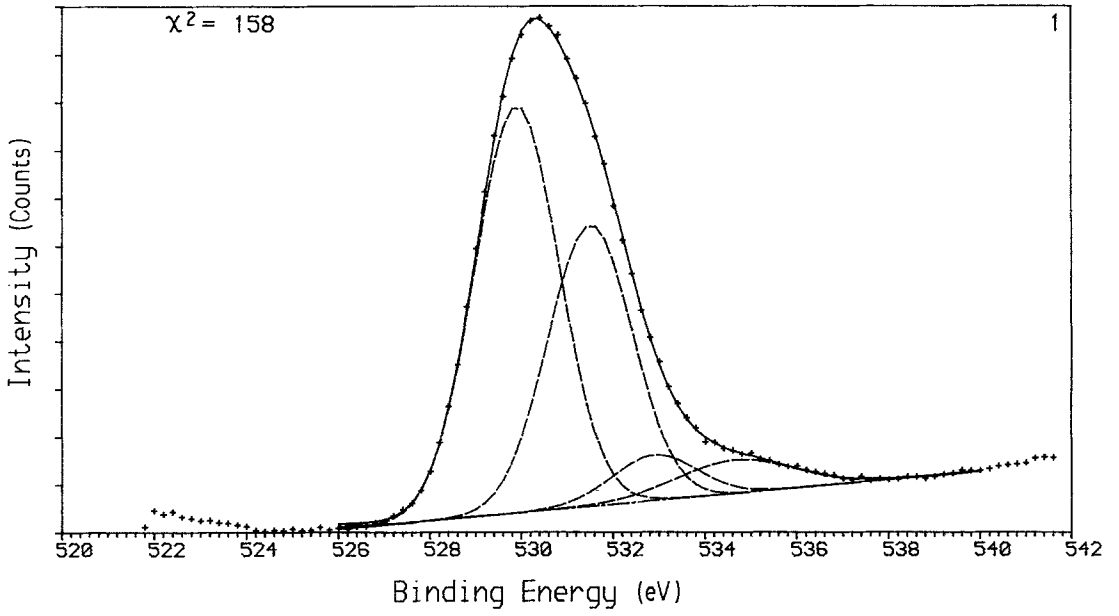

Figure 16 Substrate Ols spectrum from close to the initiating defect. Components are: (left to right) oxide, hydroxide, molecular water, Na*KLL* Auger peak.

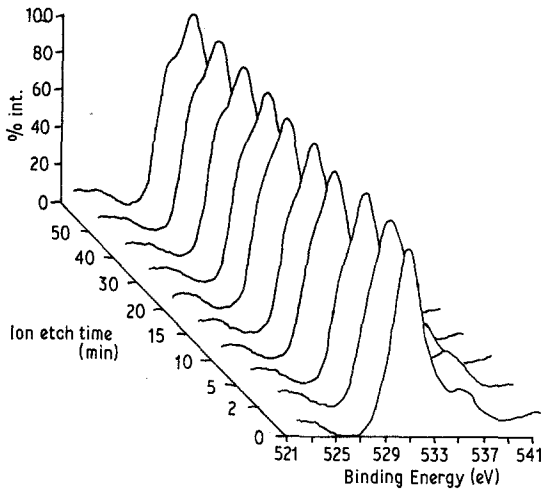

Figure 17 Ols spectrum from the substrate of a disbonded emergy abraded panel showing the development of an oxide shoulder (binding energy 530.2 eV) with increasing sputter time.

diamond-polished panel with a view to modelling the changes that occur at the interface during, and following, disbondment.

At the periphery of the disbonded zone hydroxide is dominant in the spectrum (Fig. 15). This analysis is that which is most closely indicative of the interface chemistry following disbondment. The other two specimens from this panel show up changes that occur in surface composition following disbondment. They have similar elemental composition to the periphery specimen but show a large excess of oxide over hydroxide in the Ols spectrum (Fig. 16). From this data set it can be concluded that the alkaline conditions at the periphery of the disbondment zone, present as a result of the cathodic reduction of dissolved oxygen

$$2H_2O + O_2 + 4e^- \rightarrow 4OH^-$$

are responsible for the rupture of the oxide to polymer bond. Concurrently, the outermost layers of substrate oxide are converted to hydroxide. This is also evident from the sputter depth profile of Fig. 17, the oxide becoming discernible in the spectrum after a relatively short etch time. With time, minor corrosion of the exposed substrate occurs and oxide becomes the dominant component, as in the Ols spectrum of Fig. 16. This phenomenon of oxide growth has been observed by XPS in our studies of polybutadiene on mild steel [3, 5] and by other workers using ellipsometry [10, 11].

All the chemical changes referred to above follow naturally as a consequence of oxygen reduction within a slowly extending crevice. However, this does presuppose the prior existence of a crevice as the initiating defect. Evidence for the mechanism by which the initial crevice forms is believed to be seen in the bright halo surrounding each starting defect. The extent of this halo region was independent of surface profile but was seen to vary with defect geometry. It is proposed that oxide reduction occurs (at a pH of about 13.5 [12]) in the defect at the oxide metal interface where only an air-formed oxide film is present. The reduction process continues along the oxide/metal interface until for some reason the failure path crosses to the oxide/polymer interface. In considering the processes that could be responsible for this transition, one must remember the stresses that will undoubtedly be present in the film after curing. The presence of a holiday in the film will create a different distribution of stresses in that

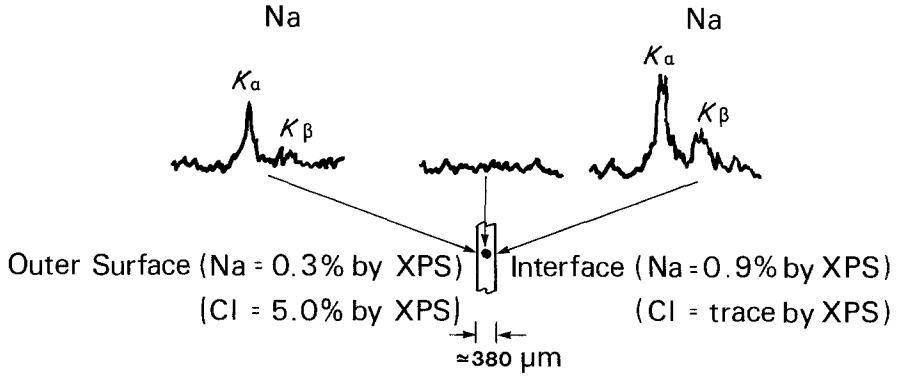

Figure 18 EPMA results obtained from a cross-section of disbonded polymer. The XPS results were obtained from pieces of the same region of polymer.

TABLE V Surface roughness values and calculated disbondment velocities Dk and $\overline{Dk}$

Surface treatment	R_a (μm)	τ	Dk (mm day^{-1})	$\overline{Dk}$*
Diamond polish	0.05	1.0	0.4, 0.6	0.50
Emery abrasion	0.85	1.6	0.4, 0.3, 0.3	0.36
Alkali clean	1.70	1.8	0.4, 0.3	0.35
Grit blast	3.80	4.7	0.4, 0.3, 0.4, 0.4, 0.4	0.38

*$\overline{Dk}$ calculated from Dk values correct to three significant figures.

part of the coating, the geometry of the defect influencing the magnitude of such a stress field. The larger the defect (or more bevelled the sides) the more gradual the change in stress distribution as the holiday is approached. As the substrate oxide is reduced in the manner described above, so such stresses are released, and a point will be reached at which the polymer "lifts" a small distance from the substrate and the fracture path passes through the oxide to the oxide/polymer interface. Thus the width of the bright halo is a function of defect geometry; a small parallel-sided defect yields a small halo (1 to 2 mm wide as observed in the majority of tests reported here). A larger, more bevelled, defect will show a much larger halo region reflecting the gradual change in stress distribution. This process of oxide reduction creates a crevice at the substrate/coating interface which allows easy access of sodium ions and the development of the high pH necessary for disbondment which is impossible at the abrupt junction between polymer and metal oxide originally present at the holiday.

Once the locus of failure passes from the oxide/metal interface to the polymer/oxide interface and hence allows alkaline attack of the polyer-to-oxide bonding, cathodic delamination occurs if the flux of hydroxyl ions is sufficient (model calculations indicate a local pH of about 11 is necessary [13]).

Thus in the initial stages the rate of delamination will be dependent on the rate of production of hydroxyl ions, which in turn is a function of the geometric area of the cathode. This reasoning may be expressed as:

$$\frac{dA}{dt} \propto \frac{d[OH]}{dt} \propto A$$

$$\frac{dA}{dt} = kA$$

$$\int_0^A \frac{dA}{A} = \int_0^t k\,dt$$

where k is a constant, area $= A$ when time $= t$.

Integrating:

$$\ln A = kt.$$

Hence a logarithmic dependence of disbondment area with time is predicted. The data of Fig. 5 show this to be the case in the intermediate stages of failure.

In the long term, however, the failure rate depends only on surface profile. In this case it should be possible to define cathodic disbondment in terms of a tortuosity related parameter. To this end we define a tortuosity factor, τ, the ratio of the actual length of the surface profilometry trace (as determined with a map measure), to the apparent length along the surface. In order to assess the ability of τ to relate to disbondment kinetics a delamination velocity (Dk) has been calculated for each disbondment test using the formula,

$$Dk = \frac{\text{disbondment radius}}{\text{disbondment time}} \times \tau \text{ mm day}^{-1}$$

Values of R_a and τ together with the individual and mean values of Dk are presented in Table V.

The mean values of Dk vary little with surface profile. This lends confidence to the notion of a constant disbondment velocity (Dk^*) for the epoxy/steel system.

The overall mean value of Dk is 0.395 mm day^{-1} and thus a value of $Dk^* = 0.40 \pm 0.08$ mm day^{-1} does not seem unreasonable. Obviously expressing a crack-propagation rate in such units is rather clumsy (although it does allow the disbondment rate to be easily envisaged), converting to the more usual SI units for such a value

$$Dk^* = 5 \pm 1 \text{ nm sec}^{-1}$$

This dependence of delamination kinetics on path length points to the final rate-controllling step being the diffusion of mobile species along the substrate/coating interface. As the epoxy is undoubtedly permeable to oxygen and water, the diffusion of sodium ions and the production and migration of hydroxyl ions along the interface will

be rate-controlling. The EPMA results of Fig. 18 show that although the epoxy film does allow diffusion of sodium ions it does so only very slowly, and will not be of any consequence within the timescale of the tests discussed in this paper. It is interesting that although the interfacial surface shows a large excess of sodium ions, the outer surface of the same sample of polymer shows an anion excess (Table IV). Both surfaces showing a much higher level of ions than the free film. One intriguing possibility is that a suble charge-balancing process is occurring across the film in the former case; the excess of sodium ions is undoubtedly a result of the underfilm alkaline conditions, this being balanced by a chloride excess on the free surface in contact with the solution.

Sodium carbonate deposits are present at the interface in the longer term tests. These are a result of carbon dioxide absorption by the test solution. An alternative explanation, favoured by Hammond *et al.* [9], is that the carbonate residues are a result of degradation of the organic cross-linking agent present in the resin, in this case such residues were apparent after a very short exposure time. We do not consider this to be the case for the work reported here as there is an "induction" period of several weeks before the carbonate precipitate becomes apparent in the XPS spectrum.

Thus the overall model for delamination can be summarised in conjunction with the kinetic data of Fig. 6. The rate-controlling step passes from oxide reduction to cathodic area (the logarithmic part of the curve), and finally to interface diffusion at time, t.

The time of transition from the intermediate stage to the final state, and the rate thereafter depends on substrate surface profile. The initial step which creates the disbondment crevice (i.e. oxide reduction) and the very early stages of delamination (Fig. 5) do not.

5. Conclusions

The rate of delamination of 3Ms 206N epoxy coating initially varies logarithmically with time, but soon approximates to a linear relationship. The magnitude of such a disbondment rate is a function of substrate surface profile, but in terms of polymer/metal oxide interfacial path length remains constant at 0.4 mm day^{-1} for all substrate pretreatments.

The earlier stages of cathodic disbondment are characterized by the reduction of the substrate oxide around the defect to a distance of 1 to 2 mm, at this point the locus of failure passes from the metal/oxide interface to the oxide/polymer junction. Here the cathodically generated underfilm alkaline environment attacks and ruptures the polymer-to-metal bonding. Hydrolysis of the substrate oxide occurs, but as the disbondment front moves radially outwards, so oxide growth is observed. Sodium carbonate may be precipitated at the interface, depending on exposure time.

The failure of epoxy-coated mild steel is predominantly adhesive, as the substrate surface profile increases, so does the proportion of cohesive failure of the oxide.

Acknowledgement

One of us (JFW) acknowledges financial support from the SERC and British Gas Corporation during the course of this work by way of a CASE Award.

References

1. British Gas Specification PS/CW6.
2. C. K. JORGENSEN and H. BERTHOU, *Discuss. Farad. Soc.* **54** (1972) 269.
3. J. E. CASTLE and J. F. WATTS, in "Corrosion Control by Organic Coatings", edited by H. Leidheiser (NACE, Houston, Texas, 1981) pp. 78–86.
4. H. LEIDHEISER and M. W. KENDIG, *Ind. Eng. Chem. Prod. Res. Dev.* **17** (1978) 54.
5. J. F. WATTS and J. E. CASTLE, *J. Mater. Sci.* **18** (1983) 2987.
6. A. B. CHRISTIE, I. SUTHERLAND and J. M. WALLS, *Vacuum* **31** (1981) 513.
7. M. GETTINGS and A. J. KINLOCH, *J. Appl. Polymer Sci.* **21** (1977) 2375.
8. D. T. CLARK and H. R. THOMAS, *J. Polymer Sci. Polymer Chem. Ed.* **14** (1976) 1671.
9. J. S. HAMMOND, J. W. HOLUBKA, J. E. DE VRIES and R. A. DICKIE, *Corros. Sci.* **21** (1981) 239.
10. J. J. RITTER and J. KRUGER, *Surf. Sci.* **96** (1980) 364.
11. *Idem*, in "Corrosion Control by Organic Coatings", edited by H. Leidheiser (NACE, Houston, Texas, 1981) pp. 28–31.
12. M. POURBAIX, "Atlas of Electrochemical Equilibria in Aqueous Solutions" (Pergamon Press, London, 1966) pp. 307–21.
13. J. F. WATTS, PhD thesis, University of Surrey (1982).

Received 23 September
and accepted 4 October 1983